ADVANCED FUNCTIONAL MATERIALS



# Recent Advances in Understanding and Development of Photorefractive Polymers and Glasses

By *Oksana Ostroverkhova*, *Daniel Wright*, *Ulrich Gubler*, *W. E. Moerner*,* *Meng He*, *Angela Sastre-Santos*, and *Robert J. Twieg*

The photoconductive, orientational, and photorefractive properties of monolithic glasses based on new nonlinear optical chromophores containing a 2-dicyanomethylene-3-cyano-2,5-dihydrofuran (DCDHF) acceptor group are presented. Large net gain coefficients are observed in both red and infrared wavelength regions. The physical and optical properties of glasses based on various DCDHF-containing derivatives are compared and analyzed, and the factors limiting steady-state and dynamical photorefractive performance are discussed.

## 1. Introduction

For many years, considerable research efforts have been directed toward exploring the interaction between light and matter for the prospective replacement of electronic devices with faster, more sensitive, and more reliable all-optical devices. Therefore, materials whose optical properties are sensitive to light, including nonlinear optical materials, have attracted attention. An important class of nonlinear optical materials is photorefractive materials in which a refractive index change is induced by non-uniform illumination via a space-charge electric field formation and the electro-optic nonlinearity.[1] These materials are of interest due to potential applications in optical data storage, optical computing, image processing, phase conjugation, and many others.[2,3] The photorefractive (PR) effect was first observed in 1969 in $LiNbO_3$ and $LiTaO_3$ crystals,[4] a discovery that launched extensive studies of the effect in inorganic materials. With the first demonstration of photorefractivity in polymers in 1991,[5] the field of organic PR materials emerged and has developed significantly since then.[6,7] PR organic materials are technologically attractive due to their low cost, ease of fabrication, and chemical tunability.[8]

The PR effect in organic materials comprises various processes such as charge photogeneration, transport, and trapping that contribute to a space-charge field formation, with a subsequent reorientation of the nonlinear optical chromophores in the space-charge field.[8,9] Due to the complex nature of the effect, the design of an "ideal" photorefractive material with good steady-state and dynamic PR performance as well as good thermal properties represents a challenge.[10,11] The reason is that characteristics of materials that are beneficial for the steady-state performance could be detrimental for both the PR dynamics and thermal stability. For example, materials possessing high dipole moments and containing high trap densities are required for the best steady-state performance. However, these properties lead to slower PR dynamics due to the increase in disorder and, as a result, decreased charge carrier mobility.[12] Also, strong dipole–dipole interactions lead to a variety of instabilities, in particular, dye aggregation,[13] crystallization and phase separation,[14,15] which shortens the material shelf life and, therefore, makes the material unsuitable for applications.

There are various approaches to creating a PR organic material.[8] The most extensively studied systems are currently polymer composites that contain photoconducting polymers (to provide a charge transport medium), sensitizing agents (to assist in charge photogeneration), nonlinear optical chromophores (to create an electro-optic response), and plasticizers (to lower the glass-transition temperature and promote the orientational enhancement effect).[6,9] In such composites substantial progress has been achieved in understanding the figures-of-merit,[9,16,17] structure–property relationships,[18] influence of relative position of HOMO levels of a sensitizer, photoconductor, chromophore, and plasticizer on charge generation,[10,19,20] transport,[10,21,22] trapping dynamics,[10,23] sample history dependence,[10,24,25] etc. The best systems reported thus far have a response time in the millisecond range[26,27] and exhibit photorefractive gain coefficients of $\sim 400\ cm^{-1}$[28] and near 100 % diffraction efficiencies[29] at applied electric fields $\sim 100\ V\,\mu m^{-1}$.

Much less explored systems include fully functionalized polymers, in which all the necessary components for the PR effect are embedded in one structure,[30–33] and multifunctional monolithic organic glasses.[34,35] Although the tunability of photorefractive properties by changing various components in

[*] Prof. W. E. Moerner, Dr. O. Ostroverkhova, Dr. D. Wright,[+] Dr. U. Gubler[++]
Stanford University, Department of Chemistry
Stanford, CA 94305 (USA)
E-mail: wmoerner@stanford.edu
M. He, Dr. A. Sastre-Santos, Prof. R. J. Twieg
Kent State University, Department of Chemistry
Kent, OH 44242 (USA)

[+] Present address: École Normale Supérieure de Cachan, ■full postal address please■, Paris, France.

[++] Second address: CSEM Alpnach, ■full postal address please■, Switzerland.

[**] The authors acknowledge the U.S. Air Force Office of Scientific Research Grant No. F49620-00-1-0038 for partial support of this work.

  1616-301X/02/0909-01 $ 17.50+.50/0 

the composite is lost, there are apparent advantages of organic glasses with respect to composites. It is known that a high concentration of the nonlinear optical chromophore is required to produce large refractive index modulations. In polymer composites, this may lead to phase separation and crystallization, which compromises the optical quality and, therefore, device performance and durability. In contrast, monolithic glasses possess large nonlinearities without stability problems due to phase separation. Also, incorporating all the functionality into a single component minimizes inert volume, which otherwise limits the change in refractive index that can be achieved. Similarly, for facile charge transport via hopping, the transporting molecules should also be present in high volume fraction. Simultaneously maximizing the volume allotted to transport and the volume allotted to nonlinearity is easily achieved with a monolithic glass based on a multifunctional molecule.

Several approaches to glass-forming low molecular weight compounds have been proposed in the literature.[36] One approach is based on utilizing the photoconductive properties of known charge-transporting moieties such as carbazole.[35] Another approach is to maximize the dipole moment ($\mu$) and polarization anisotropy ($\Delta\alpha$) to take full advantage of the orientational enhancement mechanism[9] in low $T_g$ materials.[34,37] Although high gain coefficients of up to 80 $cm^{-1}$ at 40 $V\,\mu m^{-1}$ were achieved,[36] the response times in these materials are on the order of 100 s, which is much slower than the observed response times for polymer composites that can be as low as a few milliseconds at 1 $W\,cm^{-2}$.[26,27]

Recently, our group reported a new nonlinear optical chromophore, 2-dicyanomethylene-3-cyano-5,5-dimethyl-4-(4′-dihexylaminophenyl)-2,5-dihydrofuran (abbreviated as DCDHF-6), that, when incorporated into a PVK/BBP/$C_{60}$ composite, exhibited high two-beam coupling gain coefficients of 400 $cm^{-1}$ and sub-second response times at applied electric fields of 100 $V\,\mu m^{-1}$.[28] Differential scanning calorimetry (DSC) analysis showed that the DCDHF-6 chromophore itself can form an amorphous organic glass.[38] High gain coefficients of ~150 $cm^{-1}$ at an applied field of only 25 $V\,\mu m^{-1}$ observed in DCDHF-6-based photorefractive glasses[38] prompted us to extend our exploration to a number of additional DCDHF derivatives. In this paper, we present a detailed study of several photorefractive organic glasses based on DCDHF. We analyze both steady-state and dynamical photorefractive performance of these glasses at the wavelength $\lambda = 676$ nm when sensitized with $C_{60}$ and at $\lambda = 830$ nm when sensitized with (2,4,7-trinitro-9-fluorenylidene)malonitrile (TNFM). Photoconductivity, birefringence, and chromophore reorientational mobility as well as their contribution to the photorefractive speed are discussed.

## 2. Results and Discussion

### 2.1. General Materials Properties and Thermal Properties

The chemical structures of the five DCDHF derivatives used in our studies are provided in Table 1. These five individual chromophores represent some of the general structural motifs that are being examined in a larger family. All five of these chromophores contain a dialkylamine donor group and a 2-dicyanomethylene-3-cyano-2,5-dihydrofuran acceptor group that are connected by either a benzene ring as in **1**–**4** or a styrene link as in **5**. The different alkyl groups in the amine donor are *n*-hexyl in **1**, **2**, and **4**, *n*-octyl in **3**, and 2-ethylhexyl in **5**. The length and branching in the amine donor tails mostly influence the thermal properties of these chromophores. In the acceptor portion of the chromophores the substituents at the 5-position are also varied. In chromophores **1**, **3**, and **5** there are a pair of methyl groups, in **4** there is a single methyl group and a single trifluoromethyl group, while in **5** there is a cyclic heptamethylene unit. Here again the main influence of these different groups is on the thermal properties although in the case of **4** the fluorination of the single methyl group also provides a not insignificant influence on the electronic properties by means of an inductive effect. This chromophore family is particularly interesting because the opportunity exists to systematically change structure in the acceptor heterocycle portion that is often not possible with other acceptor groups. For example, the introduction of the ring in the acceptor of **2** represents an attempt to influence the overall aspect ratio of the chromophore, which, in turn, may influence propensity for reorientation and possibly response speed. The introduction of the trifluoromethyl group in **4** represents an attempt to break the symmetry

Table 1. Optical and thermal properties of DCDHF derivatives.

| 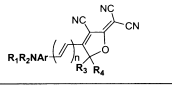 | Compound | $\lambda_{max}$ (THF) [nm] | $\varepsilon_{max}$ [L $cm^{-1}$ $mol^{-1}$] | $T_g$ [a] [°C] | $M_p$ [b] (DSC) [°C] | $T_{rec}$ [a] [°C] | $T_d$ [c] (TGA) [°C] |
|---|---|---|---|---|---|---|---|
| 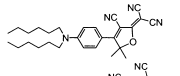 | DCDHF-6 (**1**) | 491 | 72 500 | 19 | 129 | 91 | 320 |
| 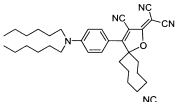 | DCDHF-6-C7M (**2**) | 492 | 74 700 | 33 | 150 | 99 | 318 |
| 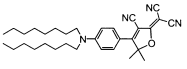 | DCDHF-8 (**3**) | 492 | 76 700 | 1 | 123 | 78 | 322 |
| 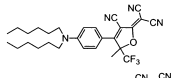 | DCDHF-6-CF3 (**4**) | 520 | 75 800 | 17 | 130 | Stable | 310 |
| 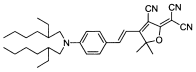 | DCDHF-2EH-V (**5**) | 574 | 50 900 | 29* | 100 | Stable* | 309 |

[a] $T_g$ and $T_{rec}$ are determined by heating samples at 10 °C $min^{-1}$ that had been previously melted and then quenched to glasses at different rates. The quench rate is 10 °C $min^{-1}$ unless the value is underlined (5 °C $min^{-1}$) or accompanied by an asterisk (30 °C $min^{-1}$). [b] $M_p$ is determined by heating a new solvent-crystallized sample at 10 °C $min^{-1}$. The recrystallization from a glass phase is often observed when a glassy sample is heated (again at 10 °C $min^{-1}$), continued heating will melt the sample again (usually, but not always, at $M_p$). [c] $T_d$, the decompostion temperature, is determined from a combination of DSC and TGA events.

  1616-301X/02/0909-02 $ 17.50+.50/0 

of the molecule and perhaps favorably influence the glass properties. At this juncture it is premature to conjecture about any general influences or combination of influences due to these structure changes. A more comprehensive study of specific structure–property relationships is underway and will be reported elsewhere.

The glass-transition temperatures ($T_g$), melting points ($M_p$), re-crystallization, and decomposition temperatures ($T_{rec}$ and $T_d$, respectively) of the glasses used in our studies are also reported in Table 1. Although many DCDHF derivatives studied can form a glassy state, amongst the compounds studied here only **4** and **5** formed a stable glass that did not crystallize over the time frame of four months so far. All other glasses were thermodynamically unstable and eventually crystallized over a period of 2–8 weeks depending on the chromophore. Also, the glassy state in these chromophores could usually only be achieved when the melt is cooled with a rate faster than 5 °C min$^{-1}$. This is illustrated in Figure 1, which shows the modulated differential scanning calorimetry (MDSC) curves obtained for DCDHF-6 as a function of cooling rate. Since

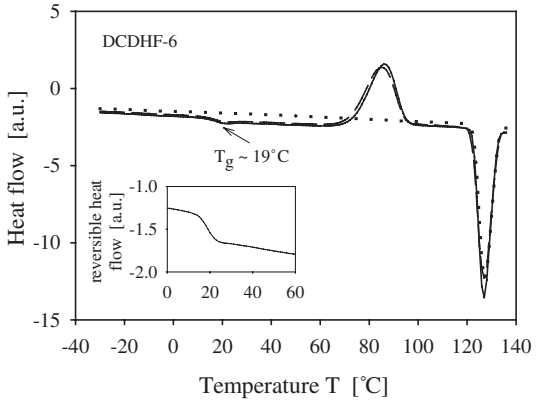


Fig. 1. Modulated differential scanning calorimetry curves of DCDHF-6 (**1**) upon heating. For fast (10 °C min$^{-1}$ (dashed line) and 20 °C min$^{-1}$ (solid line)) cooling of the melted samples, glass-like behavior ($T_g$ = 19 °C) is observed with an irreversible exothermic crystallization peak at 85 °C. For slow cooling (5 °C, dotted line), the sample is crystalline, and only the endothermic melting peak at 128 °C is visible. The inset displays the region around $T_g$. Reprinted with permission from [38].

this thermal behavior imposes strict sample preparation conditions, we investigated possible ways of stabilizing the glassy state. We found that if pairs of chromophores were mixed together with 1:1 weight ratio, a stable glass could be achieved in some cases. Two such mixtures, DCDHF-6/DCDHF-6-C7M (mixture **6**, $T_g$ ~ 23 °C) and DCDHF-8/DCDHF-6-C7M (mixture **7**, $T_g$ ~ 20 °C), were prepared and characterized.

### 2.2. Optical Properties

Absorption spectra of chromophores **1**, **4**, and **5** are presented in Figure 2. The spectra of **2** and **3** (not shown) were found to be almost identical to that of **1**. The wavelengths at which the absorption maximum occurs ($\lambda_{max}$) as well as the molar absorption coefficients ($\varepsilon_{max}$) obtained for chromophores **1-5** dissolved in tetrahydrofuran (THF) are shown in Table 1. The structures of **1**, **2**, and **3** are very similar except for some changes in the aliphatic content on the donor and acceptor portions of the chromophores and the absorption spectra differ little. In the case of **4** the introduction of the trifluoromethyl group enhances the electron deficiency of the acceptor group and the absorption maximum is red shifted by about 30 nm. In the case of chromophore **5** the extension of the conjugation system by a single double bond results in a red shift of about 80 nm.

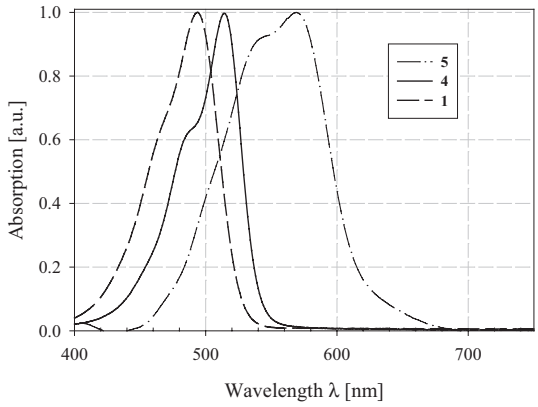


Fig. 2. Normalized absorption spectra of DCDHF-6 (**1**), DCDHF-6-CF3 (**4**), and DCDHF-2EH-V (**5**) in chlorobenzene.

All glasses, except for **5**, yield low absorption coefficients at the wavelengths $\lambda$ = 676 nm and $\lambda$ = 830 nm. This makes them good candidates for photorefractive (PR) studies in the red (upon $C_{60}$ sensitization) as well as the near-infrared (upon TNFM sensitization) wavelength region since the absorption in the sensitized compounds is mostly due to the sensitizer, which is the optimal situation for a PR organic material.[8] Indeed, the glasses **1**–**4**, **6**, and **7** sensitized with 0.5 wt.-% $C_{60}$ or with 0.5 wt.-% TNFM yielded similar absorption coefficients ($\alpha$) of 9–22 cm$^{-1}$ at $\lambda$ = 676 nm and $\lambda$ = 830 nm respectively, as indicated in Table 2. Glass **5** sensitized with 0.5 wt.-% TNFM was used in our PR experiments at $\lambda$ = 830 nm, although even at this wavelength the absorption coefficient measured in these samples ($\alpha$ ~ 114 cm$^{-1}$) was rather high due to absorption tail observed in this more highly conjugated compound (Fig. 2). This provides undesirable background absorption, which in this material counteracted the rather high PR gain coefficient ($\Gamma$), so that fields above 50 V μm$^{-1}$ were required to achieve net gain ($\Gamma$–$\alpha$).

### 2.3. Photoconductive Properties

The first step in the PR grating formation is the creation of a space-charge field under non-uniform illumination. This process is governed by photoconductivity, which is a complex characteristic that combines charge carrier photogeneration, drift mobility, trapping, and recombination.[10] The rates describing these processes determine the dynamics of space-charge field formation as well as the maximal space-charge field achievable in a given material under certain conditions.[10,11] In the sim-

  1616-301X/02/0909-03 $ 17.50+.50/0 

Table 2. Photoconductive, orientational and photorefractive properties of DCDHF-based glasses.

| Compound | $\alpha_{676}$ [cm$^{-1}$] | $\alpha_{830}$ [cm$^{-1}$] | $\Gamma_{676}$ [a] [cm$^{-1}$] | $\Gamma_{830}$ [b] [cm$^{-1}$] | $\tau_g^{-1}$ [c] [s$^{-1}$] | Fan loss [d] [%] | $\sigma_{dark}$ [e] [pS/cm] | $\sigma_{ph}$ [f] (676nm) [pS/cm] | $k_{BR}$ [g] [s$^{-1}$] | $\kappa_r$ [h] [s$^{-1}$] | $\kappa_d$ [i] [s$^{-1}$] |
|---|---|---|---|---|---|---|---|---|---|---|---|
| **1**/$C_{60}$ | 12.7 | – | 173 | – | 0.6 | 17 | 0.08 | 1.75 | 0.4 | 0.41 | 0.002 |
| **2**/$C_{60}$ | 12.9 | – | 41 | – | 0.061 | 4 | 0.1 | 1.25 | 0.021 | 0.06 | 0.032 |
| **3**/$C_{60}$ | 19.2 | – | 57 | – | 1.22 | – | – | – | 68 | 2 | 1.4 |
| **4**/$C_{60}$ | 19.9 | – | 149 | – | 0.116 | 2 | 0.07 | 0.56 | 1.3 | 0.21 | 0.027 |
| **6**/$C_{60}$ | 12.2 | – | 158 | – | 0.022 | 28 | 0.13 | 2.17 | 0.03 | 0.016 | 0.0015 |
| **7**/$C_{60}$ | 16.3 | – | 93 | – | 0.126 | 18 | 0.04 | 2.4 | 1.2 | 0.56 | 0.005 |
| **1**/TNFM | – | 9.2 | – | 129 | 0.12 | 2 | – | – | – | – | – |
| **4**/TNFM | – | 21.8 | – | 27 | 0.007 | – | – | – | – | – | – |
| **5**/TNFM | – | 113.6 | – | 76 | 0.088 | – | – | – | 0.025 | – | – |
| **6**/TNFM | – | 10.8 | – | 117 | 0.005 | – | – | – | – | – | – |
| **7**/TNFM | – | 10.4 | – | 49 | 0.018 | – | – | – | – | – | – |

[a] Wavelength $\lambda = 676$ nm, electric field $E = 25$ V μm$^{-1}$, total writing intensity $I = 100$ mW cm$^{-2}$. [b] $\lambda = 830$ nm, $E = 45$ V μm$^{-1}$, $I = 100$ mW cm$^{-2}$. [c] $C_{60}$-sensitized compounds: $\lambda = 676$ nm, $E = 20$ V μm$^{-1}$, $I = 100$ mW cm$^{-2}$; TNFM-sensitized compounds: $\lambda = 830$ nm, $E = 45$ V μm$^{-1}$, $I = 100$ mW cm$^{-2}$. [d] $E = 30$ V μm$^{-1}$, $I = 100$ mW cm$^{-2}$. [e] $E = 20$ V μm$^{-1}$. [f] $E = 20$ V μm$^{-1}$, $I = 25$ mW cm$^{-2}$. [g] $E = 20$ V μm$^{-1}$. [h] $\lambda = 676$ nm, $E = 20$ V μm$^{-1}$, $I = 800$ mW cm$^{-2}$. [i] $\lambda = 676$ nm, $E = 20$ V μm$^{-1}$.

plest PR model developed for inorganic crystals, the rate of space-charge field formation ($k_{SC}$) has the simple relationship to the photoconductivity[1] ($\sigma_{ph}$): $k_{SC} \sim \sigma_{ph}/(\varepsilon\varepsilon_0)$, with $\varepsilon_0$ and $\varepsilon$ being the electric permittivity of vacuum and dielectric constant, respectively. Although in organic materials the relationship between $k_{SC}$ and $\sigma_{ph}$ is more complicated than in inorganic crystals due to a strong electric field dependence of charge generation and drift mobility,[10,39] the proportionality of $k_{SC}$ and $\sigma_{ph}$ still holds. Thus, similar incident light intensity dependencies of $k_{SC}$ and $\sigma_{ph}$ are expected.[26] Therefore, if the PR grating formation speed is limited by the space-charge field dynamics, i.e., photoconductivity, rather than chromophore reorientation, then both the PR speed and photoconductivity should similarly depend on incident light intensity.

The incident light intensity dependence of photoconductivity observed in samples **1**, **2**, **4**, **6**, and **7** sensitized with $C_{60}$ at an electric field of 20 V μm$^{-1}$ at the wavelength $\lambda = 676$ nm is shown in Figure 3. Comparing the photoconductivities of all the compounds at a light intensity of ~10 mW cm$^{-2}$, we note that the samples **1**/$C_{60}$, **6**/$C_{60}$ and **7**/$C_{60}$ possess approximately equal values of photoconductivity, while the photoconductivity of the samples **2**/$C_{60}$ and **4**/$C_{60}$ is lower. Since carrier drift mobility depends on the temperature relative to $T_g$, the higher $T_g$ of the sample **2**/$C_{60}$ ($T_g = 33$ °C) could explain the lower photoconductivity in this compound.[11,40] The lower photoconductivity in the compound **4**/$C_{60}$ could be attributed to a higher ionization potential of chromophore **4** ($I_p = 5.61$ eV) in comparison with that of chromophore **1** ($I_p = 5.56$ eV) that leads to a reduced charge photogeneration efficiency.[20]

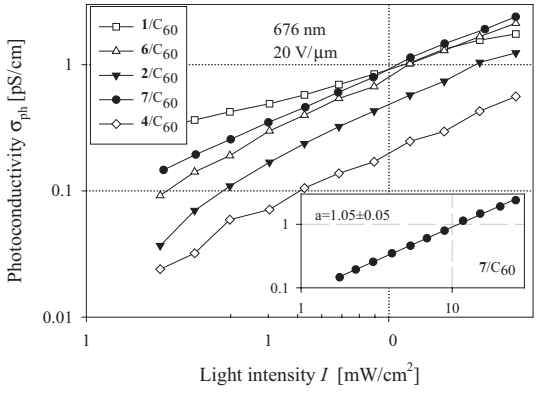


Fig. 3. Photoconductivity obtained in the compounds **1**/$C_{60}$, **2**/$C_{60}$, **4**/$C_{60}$, **6**/$C_{60}$ and **7**/$C_{60}$ at $\lambda = 676$ nm with an electric field of 20 V μm$^{-1}$ as a function of light intensity. The inset shows the power law fit $\sigma \sim I^a$, performed in the compound **7**/$C_{60}$, with the exponent $a$ close to 1.

In most compounds, the dark conductivity was at least an order of magnitude smaller than the photoconductivity at light intensities above 10 mW cm$^{-2}$ at a given applied electric field. The dark conductivity and photoconductivity values measured at an electric field of 20 V μm$^{-1}$ and incident light intensity of 25 mW cm$^{-2}$ are summarized in Table 2.

It is possible that charge transport in these types of glass depends on the microscopic morphology that could be affected by the thermal history of the sample, namely, cooling rate during the sample preparation. Nevertheless, all glasses exhibited almost a linear intensity dependence of the photoconductivity ($\sigma_{ph}$), with the exponent $a$ of the power law $\sigma_{ph} \sim I^a$ ranging between 0.9 and 1.1. The inset of Figure 3 illustrates the power law fit for the compound **7**/$C_{60}$, which yields the exponent $a = 1.05 \pm 0.05$. Compared to PVK/$C_{60}$-based photorefractive composites, the photoconductivities of DCDHF/$C_{60}$ glasses are of the same order of magnitude,[26] which suggests similar charge redistribution rates in these two classes of materials.

### 2.4. Birefringence

To evaluate the size of the potential nonlinear optical response as well as to probe orientational mobility of the chromophores, we performed transient ellipsometry experiments. Figure 4 shows the time evolution of the refractive index change due to the chromophore orientation in the external electric field of 25 V μm$^{-1}$ at room temperature (RT) of ~21 °C. For convenient comparison of the dynamics, the birefringence ($\Delta n$) is normalized by the values obtained at a time $t = 100$ s after the electric field was turned on ($\Delta n_{100}$). The rise of the birefringence $\Delta n$ was fitted to either a single exponential ($\Delta n \sim C[1-\exp(-k_{BR}t)]$ with $C$ a constant) or stretched exponential function ($\Delta n \sim C[1-\exp(-k_{BR}t)^{\beta}]$). Single exponential behavior at RT was characteristic of glasses with glass-transition temperatures ($T_g$) below RT. These included compounds

  1616-301X/02/0909-04 $ 17.50+.50/0 

ADVANCED FUNCTIONAL MATERIALS



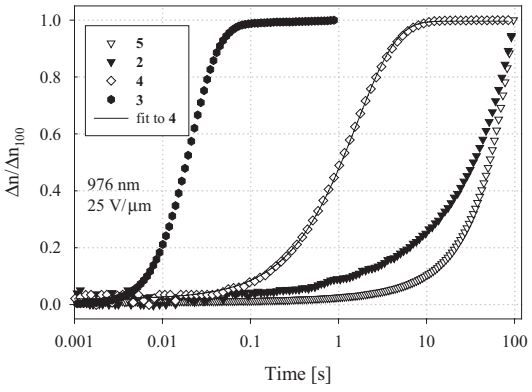


Fig. 4. Transient behavior of electric field-induced birefringence in the compounds **2**/$C_{60}$, **3**/$C_{60}$, **4**/$C_{60}$, and **5**/$C_{60}$. The orientational dynamics appears over several orders of magnitude in time depending on the $T_g$ of the glass. The solid curve illustrates a single exponential fit to the data for compound **4**.

**1**, **3**, **4**, and **7**. Glasses with a $T_g$ above RT (compounds **2**, **5**, and **6**) showed more dispersive behavior, with the parameter $\beta = 0.46 \pm 0.01$ ($\beta = 1$ corresponds to no dispersion) and much slower chromophore orientational mobility (Fig. 4). Decay transients exhibited similar behavior to rise transients, but with faster response times. This could be evidence that the Debye rotational diffusion model,[41] which describes the reorientation of a rigid dipolar molecule in an isotropic medium, approximates the orientational processes in our materials well.[42]

The orientational mobilities characterized by the coefficient $k_{BR}$ introduced above for the glasses studied are presented in Table 2. As is apparent from Figure 4 and Table 2, the relative value of $T_g$ with respect to RT crucially affects the chromophore orientational mobility, and several orders of magnitude improvement in orientational speed could be achieved by adjusting the $T_g$ of the chromophore or ambient temperature. The study of temperature dependence of various processes in the DCDHF glasses is currently in progress and will be reported elsewhere.

Figure 5 shows the dependence of the refractive index change ($\Delta n$) on the electric field. For several compounds (**1**, **3**, **4**, and **7**), the values of $\Delta n$ plotted in Figure 5 represent the steady-state values. For compounds in which the transients did not level off within the duration of our experiment, the refractive index change ($\Delta n$) was evaluated at time $t =$ 100 s after the electric field was turned on ($\Delta n_{100}$). The $\Delta n_{100}$ in most of our compounds are among the best values reported,[16] reaching nearly $10^{-2}$ at an electric field of 30 V μm$^{-1}$ at a far-from-resonance wavelength $\lambda = 976$ nm.

In most compounds, the birefringence values $\Delta n_{100}$ were found to follow an almost quadratic dependence on the electric field at fields $E < 30$ V μm$^{-1}$, as expected for Kerr orientation.[43] As an illustration, the power law fit $\Delta n \sim E^b$ performed for the compound **6**/$C_{60}$ that yields the exponent $b = 1.92 \pm 0.10$, is shown in the inset of Figure 5. However, in the compound **7**/TNFM, the birefringence leveled off at an electric field of ~25 V μm$^{-1}$ that indicates the saturation of electric field-induced molecular re-arrangement in this glass.

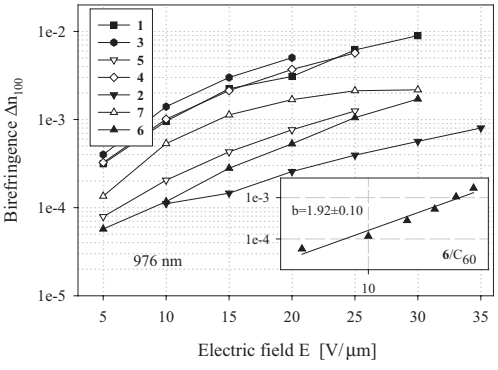


Fig. 5. Birefringence of **1**–**7**/$C_{60}$ compounds evaluated at time $t = 100$ s after the electric field of 20 V μm$^{-1}$ is applied. The solid lines are guides to the eye. The inset shows the power law fit $\Delta n \sim E^b$, performed in the compound **6**/$C_{60}$, with the exponent $b$ indicating almost quadratic dependence.

## 2.5. Photorefractive Properties

### *2.5.1. At 676 nm*

The photorefractive gain coefficient for $C_{60}$-sensitized glasses at the wavelength of 676 nm as a function of applied electric field is shown in Figure 6. In particular, Figure 6a illustrates the PR performance of the compounds **1**–**4**/$C_{60}$, while Figure 6b depicts the gain coefficients in the samples made from mixtures **6**/$C_{60}$ and **7**/$C_{60}$. Out of the compounds **1**–**4**/$C_{60}$, only **4**/$C_{60}$ was thermally stable. Therefore, by performing PR

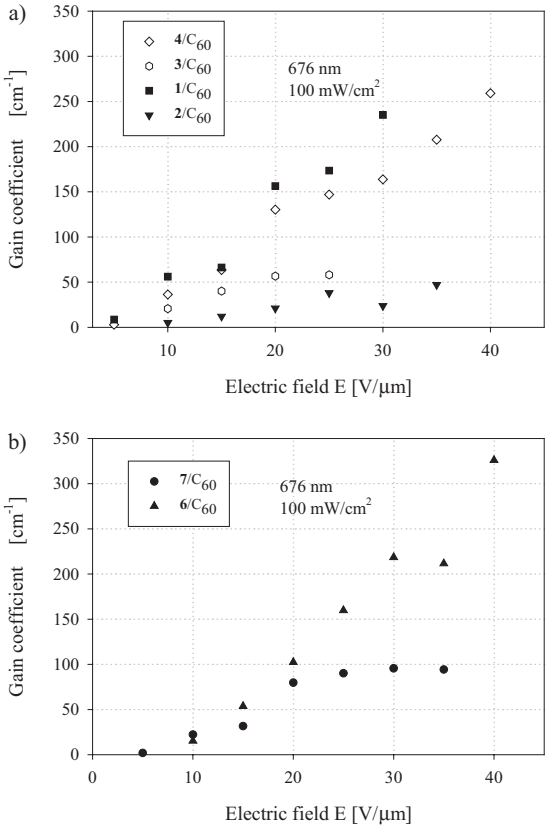


Fig. 6. Gain coefficient of $C_{60}$-sensitized compounds as a function of electric field at the wavelength of 676 nm, 1:1 beam ratio, and 100 mW cm$^{-2}$ total writing beam intensity in: a) "pure" compounds **1**–**4**/$C_{60}$; b) mixtures **6**/$C_{60}$ and **7**/$C_{60}$.

  1616-301X/02/0909-05 $ 17.50+.50/0 

experiments on chromophore mixtures **6**/$C_{60}$ and **7**/$C_{60}$ that form a stable glass, we sought good thermal properties combined with high gain coefficients. Indeed, the mixture **6**/$C_{60}$ exhibited gain coefficients as high as those of the best "pure" compound **1**/$C_{60}$. However, the dynamical PR performance worsened due to increased $T_g$ and, possibly, complicated molecular arrangement in the bulk that hindered re-orientation. The thermally stable mixture **7**/$C_{60}$ is characterized by a reasonable PR response time for the DCDHF glasses that will be discussed further in the text. However, the gain coefficient in this material is ~100 $cm^{-1}$ at an electric field of 30 V $\mu m^{-1}$ (Fig. 6b), which is below the gain coefficients observed in other DCDHF derivatives.

Several glasses exhibited net gain coefficients as high as 200 $cm^{-1}$ at electric fields of ~30 V $\mu m^{-1}$, which is the best value reported so far at such low electric fields. Since the requirement of high applied electric fields is one of the major materials concerns for photorefractive organic materials, the DCDHF-based glasses described here represent a significant improvement in material design since the net gain in these materials is achieved at an electric field as low as 5 V $\mu m^{-1}$. The gain coefficients achieved at an electric field of 25 V $\mu m^{-1}$ are summarized in Table 2. An error in gain coefficients (Table 2) was ~10 % as estimated from the spread of values observed in different samples made of the same compound. Although the two-wave mixing experiments were conducted under conditions minimizing the beam fanning effect[44] and separating time scales of the beam coupling and fanning,[38] strong fanning prevented the PR measurements at electric fields higher than 30–40 V $\mu m^{-1}$ depending on the material.

The PR response speed, defined as the inverse time constant ($\tau_g^{-1}$) obtained by single exponential fits of the gain[26] observed at an applied electric field of 20 V $\mu m^{-1}$ and total incident intensity of 100 mW $cm^{-2}$, is shown in Table 2. As seen in Table 2, the response speed $\tau_g^{-1}$ is quite slow, ranging from 0.06 to 1.2 $s^{-1}$ depending on the compound. Although $\tau_g^{-1}$ is an important characteristic for applications that utilize the beam coupling properties of the PR material, the dynamics of the refractive index change is assessed more directly using the four-wave mixing geometry.[7] Therefore, to probe the dynamics of grating formation and erasure, we performed a degenerate four-wave mixing (DFWM) experiment. The grating dynamics was described by either a single exponential function ($\eta \sim \sin^2[C(1-\exp(-\kappa_r t))]$ for rise or $\eta \sim \sin^2[C\exp(-\kappa_e t)]$ for erasure) or a stretched exponential ($\eta \sim \sin^2[C(1-\exp(-(\kappa_r t)^{\beta}))]$ or ($\eta \sim \sin^2[C\exp(-(\kappa_e t)^{\beta})]$). The parameters $\kappa_r$ and $\kappa_e$ are taken to be characteristic of the PR dynamical performance and referred to as the PR rise and erasure speed, respectively. The experiment was performed as a function of total writing beam intensity, in the case of grating formation, or erasing beam intensity, in the case of grating decay.

We found that in all of our compounds both the rise and erase PR speed had a sublinear intensity dependence, which in our case is an indication of PR speed being limited by chromophore orientation.[26] Figure 7 shows the PR erase speed $\kappa_e$ as a function of erasing beam intensity obtained at an electric field of 20 V $\mu m^{-1}$ in the chromophores **4**, **6**, and **7** sensitized with $C_{60}$. In mixtures **6**/$C_{60}$ and **7**/$C_{60}$, the PR erase speed $\kappa_e$ saturated at a light intensity of ~70 mW $cm^{-2}$ at values ~0.02 and 0.18 $s^{-1}$ respectively. Although $\kappa_e$ of the compound **4**/$C_{60}$ did not saturate in the intensity range studied, the intensity dependence of $\kappa_e$ is clearly sublinear.

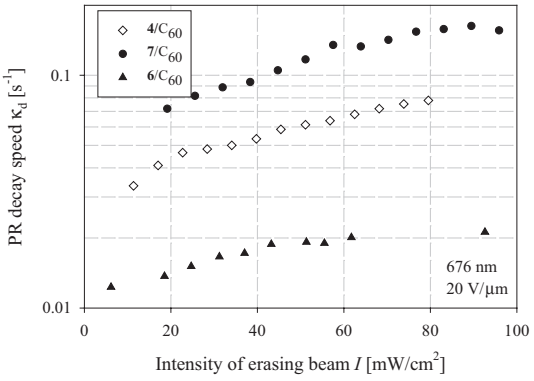


Fig. 7. PR grating erasure speed $\kappa_e$ as a function of erasing beam intensity obtained in DFWM experiment at the wavelength of 676 nm and electric field of 20 V $\mu m^{-1}$.

The PR speed determined from the DFWM experiment describes the time evolution of the refractive index change and, therefore, can be directly compared with the orientational rate constant $k_{BR}$ introduced in Section 2.4. The PR rise speed $\kappa_r$ obtained for several compounds from the single or stretched exponential fits of the diffraction efficiency transients at an electric field of 20 V $\mu m^{-1}$ and total writing beam intensity 800 mW $cm^{-2}$ is summarized in Table 2. The fact that the PR rise speed values $\kappa_r$ for the compounds **1**/$C_{60}$, **2**/$C_{60}$, **6**/$C_{60}$, and **7**/$C_{60}$ are similar to the orientational rate constants $k_{BR}$ determined by transient ellipsometry (Table 2) supports the conclusion that PR speed in these glasses is orientationally limited. The PR speed of the compounds **3**/$C_{60}$ and **4**/$C_{60}$ is considerably below the orientational rate constant, and, thus, at the intensity range studied it could be limited by photoconductivity. However, the intensity dependence of $\kappa_r$ in these compounds is also sublinear and, therefore, the saturation of the PR speed at values similar to $k_{BR}$ could occur at higher intensities.

The grating dark decay provides information about the average shallow trap depth relative to the transport manifold.[23,45] In polymer composites shallow traps are attributed to chromophores[23] or to impurities in the photoconductive polymer.[10,11] In our glasses dark decay may elucidate the degree of energetic and positional disorder in the glass itself. Values for the dark decay constant $\kappa_d$ were extracted from fits to the FWM signal in a manner similar to that for the erasure case described above. The dark decay speed $\kappa_d$ obtained for several compounds is presented in Table 2. The dark decay speed varied over three orders of magnitude, which could be evidence that the shallow traps in DCDHF-based glasses are morphological. For example, the compound **3**/$C_{60}$ ($T_g$ = 1 °C) exhibited much faster dark decay ($\kappa_d$ = 1.4 $s^{-1}$) than the chemically similar compound **1**/$C_{60}$ ($T_g$ = 19 °C, $\kappa_d$ = 0.002 $s^{-1}$), which we attribute to much higher orientational freedom in the compound **3**/$C_{60}$ which reduces effective trap depth. However, the $T_g$ is not the only factor that affects the shallow trap depth as seen from the

  1616-301X/02/0909-06 $ 17.50+.50/0 

ADVANCED FUNCTIONAL MATERIALS



comparison between the dark decay speed of compounds **1**/$C_{60}$ ($T_g = 19\,°C$, $\kappa_d = 0.002\ s^{-1}$) and **2**/$C_{60}$ ($T_g = 33\,°C$, $\kappa_d = 0.032\ s^{-1}$), which suggests the possible influence of the molecular arrangement in the bulk on the trap properties.

*2.5.2. At 830 nm*

Two-wave mixing experiments conducted at the wavelength of 830 nm showed that our glasses, sensitized with TNFM, exhibit gain coefficients among the highest reported in the near IR wavelength region,[46] reaching ~170 $cm^{-1}$ at an electric field of 55 $V\,\mu m^{-1}$. Figure 8 shows the electric field dependence of the gain coefficient measured for several glasses at 830 nm. The gain coefficients observed at an electric field of

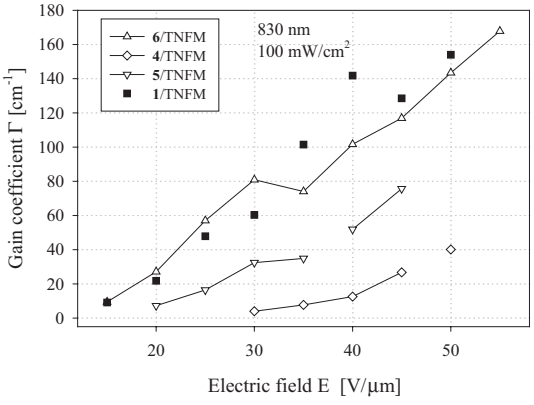


Fig. 8. Gain coefficient of TNFM-sensitized compounds as a function of electric field at the wavelength of 830 nm, beam ratio 1:1, and total incident intensity of 100 $mW\,cm^{-2}$.

45 $V\,\mu m^{-1}$ in several TNFM-sensitized compounds are shown in Table 2. Out of the five compounds studied at this wavelength, only one compound (**5**/TNFM) failed to achieve net gain ($\Gamma - \alpha > 0$) at the maximum experimental electric field of 50 $V\,\mu m^{-1}$ due to a high background absorption due to the chromophore (Fig. 2).

It is interesting to note that although chromophores **1** and **4** sensitized with $C_{60}$ were characterized by similar gain coefficients at 676 nm (Fig. 6), their performance at 830 nm is quite different, with a gain coefficient of the compound **4**/TNFM being much lower than that of **1**/TNFM. We attribute such behavior to much lower charge photogeneration efficiency (and potentially lower density of photorefractive traps) in the compound **4**/TNFM, which also affects the PR dynamics leading to a much slower PR response speed ($\tau_g^{-1}$) of **4**/TNFM (~0.007 $s^{-1}$) in comparison with $\tau_g^{-1}$ of **1**/TNFM (~0.12 $s^{-1}$).

The infrared PR response speed ($\tau_g^{-1}$) obtained from single exponential fits to the gain observed in a two-wave mixing experiment at an electric field of 45 $V\,\mu m^{-1}$ and total intensity of 100 $mW\,cm^{-2}$ is presented in Table 2. Much slower PR response was obtained in most TNFM-sensitized compounds in comparison with the orientational rate constant $k_{BR}$ defined in Section 2.4 and PR response speed $\tau_g^{-1}$ of the $C_{60}$-sensitized compounds (Table 2), suggesting that the PR speed at the wavelength of 830 nm is limited by photoconductivity. Therefore, the optimization of the compounds based on DCDHF glasses for near IR applications would include a search for a sensitizer that outperforms TNFM.

*2.5.3. Beam fanning*

Beam fanning refers to amplified light scattering in certain preferred directions observed in PR materials with high gain coefficients.[44] While there are a number of applications that rely on beam fanning for their operation,[38,44] in most devices this effect is undesirable since the amplified scatter is a source of noise. Therefore, the best performing materials for applications such as image processing or holographic data storage would ideally have the beam fanning effect minimized. Although the amount of optical scattering in the sample can be reduced by improving sample preparation techniques, the material composition can also be crucial. The power loss due to beam fanning can be measured by monitoring the power of the beam transmitted through the PR sample as a function of time. The percentage of fanning-related power loss observed in several compounds for a single incident p-polarized beam of 100 $mW\,cm^{-2}$ intensity at an electric field of 30 $V\,\mu m^{-1}$ after the time $t = 100$ s is presented in Table 2. Figure 9 shows the dynamics of the transmitted power normalized by the initial value at time $t = 0$ in the compounds **1**/$C_{60}$ and **4**/$C_{60}$ at a wavelength of 676 nm, incident beam intensity of 100 $mW\,cm^{-2}$, and an electric field of 30 $V\,\mu m^{-1}$. Both glasses exhibited high gain coefficients at this wavelength (Table 2), but the fanning is drastically reduced in the compound **4**/$C_{60}$ in comparison with that of **1**/$C_{60}$, which demonstrates the utility of different chromophores in reducing fanning while maintaining high gain coefficients.

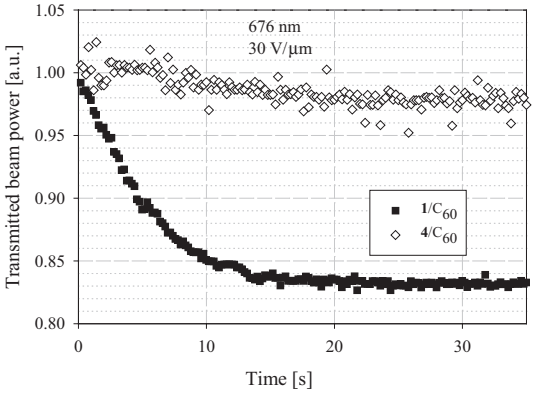


Fig. 9. Transmitted beam power loss due to beam fanning observed at 676 nm with p-polarized beam of intensity 100 $mW\,cm^{-2}$ at the electric field of 30 $V\,\mu m^{-1}$ in the compounds **1**/$C_{60}$ and **4**/$C_{60}$.

## 3. Concluding Remarks

Organic glasses containing DCDHF derivatives are new promising PR materials. They are characterized by high photoconductivity values in the red wavelength region

  1616-301X/02/0909-07 $ 17.50+.50/0 

($\sigma_{ph} \sim 1$ pS cm$^{-1}$ at a wavelength of 676 nm, electric field of 20 V μm$^{-1}$, and light intensity of ~20 mW cm$^{-2}$) and high PR beam coupling gain coefficients in both red and IR wavelength region ($\Gamma \sim 200$ cm$^{-1}$ at a wavelength of 676 nm and electric field of 30 V μm$^{-1}$, and $\Gamma \sim 150$ cm$^{-1}$ at a wavelength of 830 nm and electric field of 50 V μm$^{-1}$, respectively). However, in spite of these favorable attributes a number of issues are yet to be resolved.

One of the issues is low PR speed, which in these glasses ranges from 0.005 to 1 s$^{-1}$ depending on the material and the wavelength. The PR dynamics at a wavelength of 830 nm seems to be limited by photoconductivity, in particular, charge photogeneration efficiency, and, thus, can be improved by optimizing the sensitizer. In contrast, the PR dynamics at a wavelength of 676 nm in most glasses is limited by chromophore orientation. The orientational mobility can be improved by several orders of magnitude by adjusting the glass-transition temperature of the compound, which provides a great potential for improving the PR speed, a concept that is currently under detailed study.

Another issue in these materials is strong beam fanning, which can be minimized by improving design, fabrication, and purity of the materials. Reduced beam fanning would allow utilization of the extraordinary high gain coefficients that would be available at higher electric fields (> 50 V μm$^{-1}$), which are inaccessible in current materials.

In addition to photoconductive and PR properties of DCDHF-based glasses, the thermal stability remains a concern. The compound **6**/$C_{60}$, which is the 1:1 (w/w) mixture of thermally unstable glasses **1**/$C_{60}$ and **2**/$C_{60}$, formed a stable glass that exhibited gain coefficients as high as the compound **1**/$C_{60}$. However, the PR speed ($\kappa_r$) obtained in the mixture **6**/$C_{60}$ is reduced more than an order of magnitude in comparison with that of **1**/$C_{60}$ (0.41 and 0.016 s$^{-1}$, respectively). The best thermally stable glass that possessed high gain coefficients ($\Gamma \sim 260$ cm$^{-1}$ at the wavelength of 676 nm and the electric field of 40 V μm$^{-1}$) while retaining a PR speed ~0.2 s$^{-1}$ and comparatively low beam fanning, was DCDHF-6-CF3 containing glass **4**/$C_{60}$. However, the near IR PR performance of the DCDHF-6-CF3 based glass is yet to be improved by replacing TNFM with a better sensitizer.

In summary, we have presented a detailed study of the thermal, photoconductive, orientational, and photorefractive properties of several DCDHF-containing organic glasses. Considering the high performance available from several of these materials and the demonstrated ability to change various properties by rational materials design, the promise of this class of materials for future applications is quite good.

## 4. Experimental

*Synthesis*: A representative synthesis of the benzene-linked chromophores such as **1**–**4** is provided in the literature [38]. The synthesis of the styrene-linked chromophores such as **5** follows from a published method [47]. Chromophores with the same heterocycle acceptor group have found wide use in electro-optic materials [48]. Full details of the synthetic procedures will be published separately.

*Cyclic voltammetry*: Oxidation potentials were determined by cyclic voltammetry. Working and auxiliary electrodes were Pt, the reference electrode was $Hg/HgCl_2$/NaCl, the supporting electrolyte was 0.1 M tetraethylammonium tetrafluoroborate in acetonitrile, and the scan rate was 300 mV s$^{-1}$. The HOMO values were calculated [49] from the oxidation potential versus the internal standard ferrocene/ferrocenium (Fc). The HOMO value for internal standard Fc is considered to be –4.8 eV.

*Sample Preparation*: The samples contained 99.5 wt.-% DCDHF chromophore and 0.5 wt.-% $C_{60}$ or TNFM depending on the wavelength region being assessed. The DCDHF chromophores and $C_{60}$ or TNFM were dissolved in chlorobenzene (50 mg mL$^{-1}$ in the case of DCDHF and 1 mg mL$^{-1}$ in the case of $C_{60}$ and TNFM), stirred, filtered through a 0.2 μm filter, and cast on the ITO slides. The films were dried overnight in an oven at 120 °C. When the residual solvent evaporated, the ITO slides with films were heated up to a temperature slightly higher than the melting point of the chromophore (125–140 °C), sandwiched with 70–120 μm spacers and quenched by placing the sample on a metal plate at room temperature. With some of the chromophores, fast cooling is crucial since otherwise they crystallize [38] instead of forming a glass. Such glasses are thermodynamically unstable and re-crystallize during the period of 2–8 weeks, depending on the material. The stable glasses maintained good optical quality over the period of at least four months.

*Absorption Spectra*: Absorption spectra of the samples were measured using a Perkin-Elmer Lambda 19 spectrophotometer. The absorption coefficients ($\alpha$) were calculated from the absorption spectra using the relation $\alpha = A/L \ln 10$, where $A$ is the decadal absorbance and $L$ is the sample thickness.

*Photoconductivity*: Photoconductivity was measured at the wavelength $\lambda = 676$ nm ($Kr^+$ laser) using a conventional DC technique [50]. First, an electric field was applied to the sample. After the transient effects disappeared (~30 s), the dark current was monitored. Then the light beam was opened with a magnetic shutter, and the current was recorded. The photocurrent was calculated as the difference between total current in the presence of light and the dark current. The dark and photoconductivity were calculated using the formula $\sigma = iL/(VS)$, where $i$ is dark or photocurrent respectively, $L$ is the sample thickness, $V$ is the applied voltage, and $S$ is the electrode area.

*Birefringence*: Electric field induced birefringence was measured using a conventional transient ellipsometry technique [51]. Light of wavelength $\lambda = 976$ nm (laser diode) was polarized at 45° with respect to the plane of incidence. The sample was placed between crossed polarizers at the angle of 54° between the sample normal and the light beam. The residual sample birefringence was compensated by a Soleil–Babinet compensator, so that no transmitted light could be detected in the absence of electric field. The electric field was applied to the sample with a rise time below 100 μs, and the intensity of transmitted light was recorded as a function of time. Then, the electric field was turned off, and the decay of the transmitted light intensity ($I$) was monitored. The birefringence was calculated using the formula

$$\Delta n = \frac{\lambda \cos\varphi}{2\pi d \sin^2\varphi} a\sin\sqrt{I/I_{max}} \quad (1)$$

where $\lambda$ is wavelength, $\varphi$ is the internal incident angle, $d$ is the sample thickness, and $I_{max}$ is the maximal transmitted intensity.

*Two-Wave Mixing*: Two-wave mixing experiments were conducted at wavelengths of 676 nm ($Kr^+$ laser) and 830 nm (laser diode). The p-polarized beams were incident at external angles of 30° and 60° to the sample normal and the beam ratio was 1:1. The total writing beam intensity was 100 mW cm$^{-2}$. The electric field was applied so that the negative high voltage would be on the sample electrode facing the incident beams. Such an experimental configuration is needed to minimize beam fanning and its related unphysical gain coefficients [44]. The beams were opened with a magnetic shutter (switching time below 150 μs), and the intensity of both amplified and depleted beams was monitored. After the measurements, the grating was erased by a larger diameter non-Bragg matched erasing beam. The gain coefficient was calculated using the formula

$$\Gamma = \frac{\cos\theta_1}{L} \ln\frac{\gamma}{2-\gamma} \quad (2)$$

where $\theta_1$ is the smaller internal angle of incidence, $L$ is the sample thickness, and $\gamma = I_{with\ pump}/I_{without\ pump}$.

*Beam Fanning*: The same setup as in the two-wave mixing experiment was used except only one beam was present. The beam was incident at the angle of 60° with respect to the sample normal, and the direction of applied electric field was inverted compared with the two-wave mixing to enhance the fanning.

*Four-Wave Mmixing*: The experiment was conducted at $\lambda = 676$ nm ($Kr^+$ laser). The grating was written by two s-polarized beams incident at external angles of 30° and 60° to the sample normal and with beam ratio 1:1. The probe beam was p-polarized, had intensity on the order of 1 % of the total writing beam intensity and was counter-propagating with one of the writing beams. The electric field was applied to the sample, the writing beams were opened with a magnetic shut-

  1616-301X/02/0909-08 $ 17.50+.50/0 

ter, and the diffracted beam was monitored as a function of time. When the diffracted signal reached a steady state, the writing beams were turned off, and either the dark decay or grating erasure in the presence of the erasing beam was recorded. Diffraction efficiency ($\eta$) was calculated as a ratio of the diffracted ($I_d$) and incident ($I_0$) probe beam intensities: $\eta = I_d/I_0$.

Received: May 27, 2002

[1] P. Yeh, *Introduction to Photorefractive Nonlinear Optics*, John Wiley, New York **1993**.
[2] J. P. Huignard, P. Gunter, *Top. Appl. Phys.* **1989**, *62*, 1.
[3] L. Solymar, D. J. Webb, A. Grunnet-Jepsen, *The Physics and Applications of Photorefractive Materials*, Clarendon Press, Oxford **1996**.
[4] F. S. Chen, *J. Appl. Phys.* **1969**, *40*, 3389.
[5] S. Ducharme, J. C. Scott, R. J. Twieg, W. E. Moerner, *Phys. Rev. Lett.* **1991**, *66*, 1846.
[6] W. E. Moerner, A. Grunnet-Jepsen, C. L. Thompson, *Annu. Rev. Mater. Sci.* **1997**, *27*, 585.
[7] S. J. Zilker, *ChemPhysChem* **2000**, *1*, 72.
[8] W. E. Moerner, S. M. Silence, *Chem. Rev.* **1994**, *94*, 127.
[9] W. E. Moerner, S. M. Silence, F. Hache, G. C. Björklund, *J. Opt. Soc. Am. B* **1994**, *11*, 320.
[10] O. Ostroverkhova, K. D. Singer, *J. Appl. Phys.* **2002**, in press.■please update if possible■
[11] T. K. Daubler, R. Bittner, K. Meerholz, V. Cimrova, D. Neher, *Phys. Rev. B* **2000**, *61*, 13 515.
[12] A. Goonesekera, S. Ducharme, *J. Appl. Phys.* **1999**, *85*, 6506.
[13] F. Wurthner, S. Yao, *Angew. Chem. Int. Ed.* **2000**, *39*, 1978.
[14] K. Meerholz, R. Bittner, Y. DeNardin, C. Brauchle, E. Hendrickx, B. L. Volodin, B. Kippelen, N. Peyghambarian, *Adv. Mater.* **1997**, *9*, 1043.
[15] E. Hendrickx, B. L. Volodin, D. D. Steele, J. L. Maldonado, J. F. Wang, B. Kippelen, N. Peyghambarian, *Appl. Phys. Lett.* **1997**, *71*, 1159.
[16] F. Wurthner, S. Yao, J. Schilling, R. Wortmann, M. Redi-Abshiro, E. Mecher, F. Gallego-Gomez, K. Meerholz, *J. Am. Chem. Soc.* **2001**, *123*, 2810.
[17] E. Hendrickx, J. Herlocker, J. L. Maldonado, S. R. Marder, B. Kippelen, A. Persoons, N. Peyghambarian, *Appl. Phys. Lett.* **1998**, *72*, 1679.
[18] K. S. West, D. P. West, M. D. Rahn, J. D. Shakos, F. A. Wade, K. Khand, T. A. King, *J. Appl. Phys.* **1998**, *84*, 5893.
[19] E. Hendrickx, Y. D. Zhang, K. B. Ferrio, J. A. Herlocker, J. Anderson, N. R. Armstrong, E. A. Mash, A. P. Persoons, N. Peyghambarian, B. Kippelen, *J. Mater. Chem.* **1999**, *9*, 2251.
[20] E. Hendrickx, B. Kippelen, S. Thayumanavan, S. R. Marder, A. Persoons, N. Peyghambarian, *J. Chem. Phys.* **2000**, *112*, 9557.
[21] G. G. Malliaras, V. V. Krasnikov, H. J. Bolink, G. Hadziioannou, *Appl. Phys. Lett.* **1995**, *66*, 1038.
[22] G. G. Malliaras, V. V. Krasnikov, H. J. Bolink, G. Hadziioannou, *Phys. Rev. B* **1995**, *52*, 14 324.
[23] A. Grunnet-Jepsen, D. Wright, B. Smith, M. S. Bratcher, M. S. DeClue, J. S. Siegel, W. E. Moerner, *Chem. Phys. Lett.* **1998**, *291*, 553.
[24] K. D. Singer, O. Ostroverkhova, *Proc. SPIE-Int. Soc. Opt. Eng.* **2001**, *4462*, 163.
[25] J. A. Herlocker, C. Fuentes-Hernandez, K. B. Ferrio, E. Hendrickx, P. A. Blanche, N. Peyghambarian, B. Kippelen, Y. Zhang, J. F. Wang, S. R. Marder, *Appl. Phys. Lett.* **2000**, *77*, 2292.
[26] D. Wright, M. A. Diaz-Garcia, J. D. Casperson, M. DeClue, W. E. Moerner, R. J. Twieg, *Appl. Phys. Lett.* **1998**, *73*, 1490.
[27] J. A. Herlocker, K. B. Ferrio, E. Hendrickx, B. D. Guenther, S. Mery, B. Kippelen, N. Peyghambarian, *Appl. Phys. Lett.* **1999**, *74*, 2253.
[28] D. Wright, U. Gubler, Y. Roh, W. E. Moerner, M. He, R. J. Twieg, *Appl. Phys. Lett.* **2001**, *79*, 4274.
[29] K. Meerholz, B. L. Volodin, Sandalphon, B. Kippelen, N. Peyghambarian, *Nature* **1994**, *371*, 497.
[30] D. Van Steenwinckel, C. Engels, E. Gubbelmans, E. Hendrickx, C. Samyn, A. Persoons, *Macromolecules* **2000**, *33*, 4074.
[31] D. Van Steenwinckel, E. Hendrickx, A. Persoons, *Chem. Mater.* **2001**, *13*, 1230.
[32] M. S. Bratcher, M. S. DeClue, A. Grunnet-Jepsen, D. Wright, B. R. Smith, W. E. Moerner, J. S. Siegel, *J. Am. Chem. Soc.* **1998**, *120*, 9680.
[33] Q. Wang, L. M. Wang, L. P. Yu, *Macromol. Rapid Commun.* **2000**, *21*, 723.
[34] P. M. Lundquist, R. Wortmann, C. Geletneky, R. J. Twieg, M. Jurich, V. Y. Lee, C. R. Moylan, D. M. Burland, *Science* **1996**, *274*, 1182.
[35] Y. D. Zhang, T. Wada, H. Sasabe, *J. Mater. Chem.* **1998**, *8*, 809.
[36] K. Meerholz, B. Kippelen, N. Peyghambarian, in *Photonic Polymer Systems* (Eds: D. Wise, G. Wnek, D. Trantolo, T. Cooper, J. Gresser), Marcel Dekker, Inc., New York **1998**.
[37] R. Wortmann, C. Poga, R. J. Twieg, C. Geletneky, C. R. Moylan, P. M. Lundquist, R. G. DeVoe, P. M. Cotts, H. Horn, J. E. Rice, D. M. Burland, *J. Chem. Phys.* **1996**, *105*, 10 637.
[38] U. Gubler, M. He, D. Wright, Y. Roh, R. Twieg, W. E. Moerner, *Adv. Mater.* **2002**, *14*, 313.
[39] J. S. Schildkraut, Y. P. Cui, *J. Appl. Phys.* **1992**, *72*, 5055.
[40] M. A. Abkowitz, M. Stolka, M. Morgan, *J. Appl. Phys.* **1981**, *52*, 3453.
[41] P. Debye, *Polar Molecules*, The Chemical Catalog Company, Inc., New York **1929**.
[42] J. Hooker, W. Burghardt, J. Torkelson, *J. Chem. Phys.* **1999**, *111*, 2779.
[43] M. Kuzyk, in *Characterization Techniques and Tabulations for Organic Nonlinear Optical Materials*, Vol. 60 (Eds: M. Kuzyk, C. Dirk), Marcel Dekker, Inc., New York **1998**.
[44] A. Grunnet-Jepsen, C. L. Thompson, R. J. Twieg, W. E. Moerner, *J. Opt. Soc. Am. B* **1998**, *15*, 901.
[45] Y. P. Cui, B. Swedek, N. Cheng, J. Zieba, P. N. Prasad, *J. Appl. Phys.* **1999**, *85*, 38.
[46] B. Kippelen, S. R. Marder, E. Hendrickx, J. L. Maldonado, G. Guillemet, B. L. Volodin, D. D. Steele, Y. Enami, Sandalphon, Y. J. Yao, J. F. Wang, H. Rockel, L. Erskine, N. Peyghambarian, *Science* **1998**, *279*, 54.
[47] G. Melikian, F. P. Rouessac, C. Alexandre, *Synth. Commun.* **1995**, *25*, 3045.
[48] C. Zhang, C. Wang, J. Yang, L. R. Dalton, G. Sun, H. Zhang, W. H. Steier, *Macromolecules* **2001**, *34*, 235.
[49] J. Pommerehne, H. Vestweber, W. Guss, R. F. Mahrt, H. Bassler, M. Porsch, J. Daub, *Adv. Mater.* **1995**, *7*, 551.
[50] A. Rose, *Concepts in Photoconductivity and Allied Problems*, Interscience Publishers, New York **1963**.
[51] R. Bittner, C. Brauchle, K. Meerholz, *Appl. Opt.* **1998**, *37*, 2843.

  1616-301X/02/0909-09 $ 17.50+.50/0 